10
3-25-92 ØSD

LBL-31248
UC-421

Lawrence Berkeley Laboratory
UNIVERSITY OF CALIFORNIA

Accelerator & Fusion Research Division

Heavy Ion Driven LMF Design Concept

E.P. Lee

August 1991

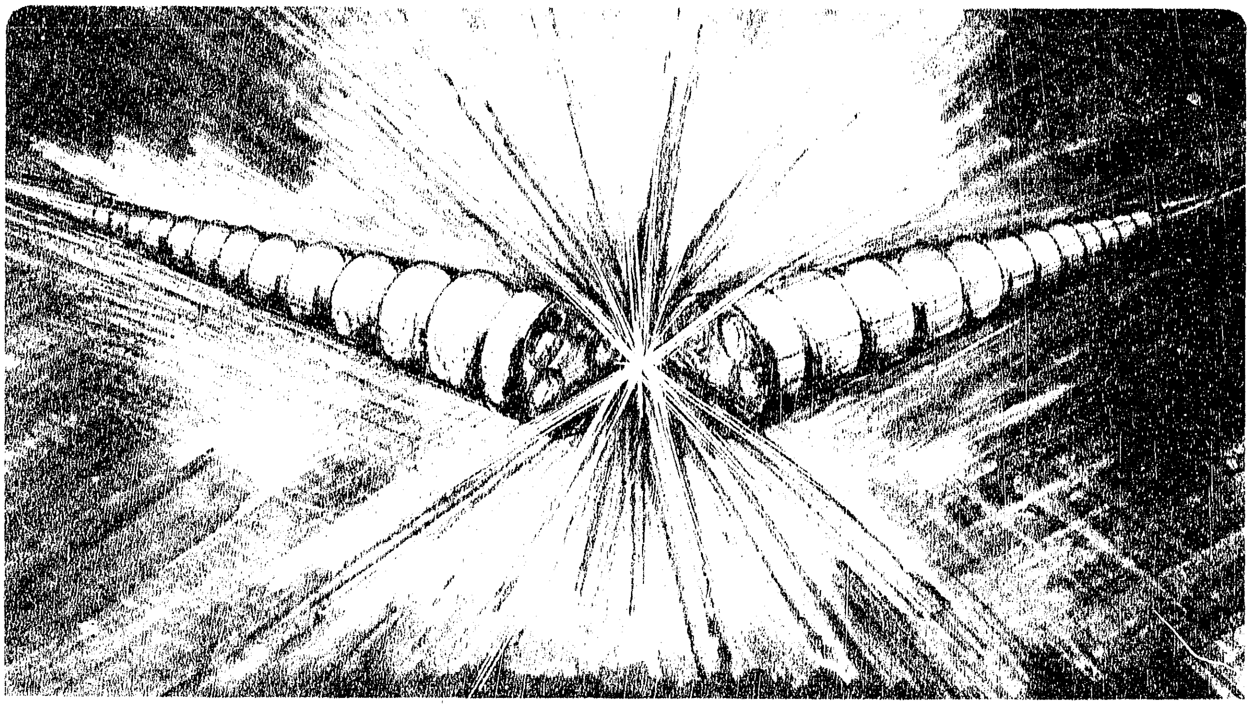

Prepared for the U.S. Department of Energy under Contract Number DE-AC03-76SF00098

LBL--31248

DE92 009489

HEAVY ION DRIVEN LMF DESIGN CONCEPT*

Edward P. Lee
Lawrence Berkeley Laboratory
1 Cyclotron Road
Berkeley, California 94720

*This work was supported by the Director, Office of Energy Research, Office of Basic Energy Sciences, Advanced Energy Projects Division, U. S. Dept. of Energy, under Contract No. DE-AC03-76SF00098.

LBL-31248
UC-421
August 1991

HEAVY ION DRIVEN LMF DESIGN CONCEPT*

Edward P. Lee
Lawrence Berkeley Laboratory
1 Cyclotron Road
Berkeley, California 94720

Introduction

The USA Department of Energy has conducted a multi-year study of the requirements, designs and costs for a Laboratory Microfusion Facility (LMF). The primary purpose of the LMF would be testing of weapons physics and effects simulation using the output from microexplosions of inertial fusion pellets. It does not need a high repetition rate, efficient driver system as required by an electrical generating plant. However there would be so many features in common that the design, construction and operation of an LMF would considerably advance the application of inertial confinement fusion to energy production. The DOE study has concentrated particularly on the LMF driver, with design and component development undertaken at several national laboratories. Principally, these are LLNL (Solid State Laser), LANL (Gas Laser), and SNLA (Light Ions). Heavy Ions, although considered a possible LMF driver, did not receive attention until the final stages of this study since its program management was through the Office of Energy Research rather than Defense Programs. During preparation of a summary report for the study it was decided that some account of heavy ions was needed for a complete survey of the driver candidates. A conceptual heavy ion LMF driver design was created for the DOE report which is titled LMC Phase II Design Concepts. The heavy ion driver did not receive the level of scrutiny of the other driver concepts and, unlike the others, no cost analysis by an independent contractor was performed. Since much of heavy ion driver design lore was brought together in this exercise it is worthwhile to make it available as an independent report. This is reproduced here as it appears (as a section) in the DOE report.

*This work was supported by the Director, Office of Energy Research, Office of Basic Energy Sciences, Advanced Energy Projects Division, U. S. Dept. of Energy, under Contract No. DE-AC03-76SF00098.

A. DESIGN OVERVIEW

1. General Features of a Heavy Ion LMF Driver

Major features of a 5 MJ, heavy ion LMF Concept are outlined in this section. Driver details are given in section B. The facility would produce 450 MJ yield from a suitable, indirectly driven target, provided other requirements on spot size, peak power, etc. are also satisfied. Most LMF objectives of weapons-physics and effects-testing can be achieved at this level. However, a 10 MJ driver with 1000 MJ yield could be realized by duplicating the 5 MJ driver and expanding the final transport and focal area. It is expected that a 5 MJ, low repetition rate system will also be a very valuable test bed for inertial fusion energy production, including target physics, chamber design, final focus and driver development. While no detailed cost breakdown is presented here, the 5 MJ driver is expected to cost about $1000 M (FY 90 dollars, direct costs, without engineering and management included), extrapolated from a previous power plant study(1). The heavy ion driver type selected for this study is the multiple-beam induction linac, which is the conservative, nearer-term option that has received the most study in the USA. Selected ion type is 2.5 GeV Kr^+ for low cost and source availability.

2. Background

A heavy ion ICF driver is recognized to be well-suited for the production of electrical power.(2) This is a result of the intrinsic high repetition rate, long life, reliability, and electrical efficiency of the accelerator. However, these features are not a priority for an LMF, which would use a few pulses on targets per day at most. Furthermore, the present level of development of heavy ion drivers is well behind that of the solid state and gas lasers as well as light-ion diodes. This difference is understandable; heavy ion fusion research has typically received only 10-20% of the funding of the other programs. This historic fact, along with a perception that a heavy ion driver's cost would be higher than that of the others, has virtually excluded it from consideration for an LMF to date. An exception is a 1987 study by Monsler(3), which examined cost reductions and scaling of major parameters achievable by modifying power plant driver designs to meet LMF objectives. In spite of this "poor cousin" status, it is desirable to include an account of heavy ions in the Phase II report for several reasons. These include completeness of the study and the value of having an alternative for comparison with the three primary candidates. Also, a basis is laid for future consideration of a heavy ion driver that incorporates evolving technical features and cost projections.

The point design presented here represents a very small effort compared with that made for the other drivers. This is partly a consequence of the location of the Heavy Ion Fusion Accelerator Research (HIFAR) Program in the DOE Office of Basic Energy Sciences rather than the Office of Inertial Fusion. There is no charter for an LMF design, which is therefore only a modification of a power plant driver design. A single driver layout is presented, which is the result of several iterations towards simplicity and compactness. No cost optimization is attempted, however several obvious cost reducing modifications from a power plant driver are made. Since this design has not been previously included in the LMF study, a cost analysis cannot be presented on the same basis as the other drivers; therefore none is given here. However, the design does include an estimate of the dimensions of some of the principal components. The calculations of major parameters are also presented in moderate detail along with design formulas.

3. Selection of Acclerator Type

Three distinct heavy ion driver accelerator types were put forward in the early days of Heavy Ion Fusion:[4] the synchrotron, the radio frequency (rf) linac, and the induction linac. The first two require storage rings to amplify ion current to the desired level, while the induction linac amplifies current during acceleration. The synchrotron was dropped from consideration early on, primarily because it was poorly matched to the desired energy and current (although it is of some value for the study of beam-matter interactions and beam dynamics, now underway at GSI Darmstadt[5] using the recently commissioned heavy ion synchrotron SIS and cooling ring ESR.) Acceleration by an rf linac was adopted by the European and Japanese programs and the HIBALL system study.[6] This is a relatively mature acceleration technology, but its technical risk for the fusion application is greatly increased by the many beam manipulations involved in transfers among linacs and storage rings. Further, the projected cost of an entire rf driver system is large, leading to the use of multiple reactor chambers in a power plant to achieve and an acceptable cost of electricity.

The induction linac driver is the primary approach pursued in the USA program at present. In its mainstream version multiple beams (N ≈ 4 - 64) are accelerated in a single, long, large diameter linac.(1) The accelerator is relatively simple in concept, but cost per volt is high. Induction linac alternatives, intended to reduce cost (but probably with increased technical risk) are the multiple pulse induction linac (7) and the recirculator(8). Due to its greater familiarity, lower risk, and lower development needs, the simple induction linac is adopted here for the LMF. The progression of heavy ion linacs leading to a fusion driver of this type is sketched in Table 1, which includes the existing LBL accelerators SBTE(9) and MBE(10), the proposed ILSE(11), and projections of large scale future machines.(12, 13)

Although no detailed comparison of the induction linac and rf linac approaches can be made here, typical power plant driver layouts for these systems (circa 1984) are shown in Figure 1. The essential distinctions between them are as follows:

(1) Acceleration with an rf linac uses a well-established technology but is limited to low currents. The induction linac uses the less established pulsed power technology, but can drive high currents through an efficient, non-resonant energy transfer.

(2) Current is increased in the rf linacs through (2 → 1) funneling operations between accelerators and the use of transfer and storage rings. An induction linac can increase current directly by pulse compression in time. Beam combination may also be employed. These operations are not well-developed for either approach at the relevant currents.

(3) The outward appearance of simplicition of the induction linac is probably offset by the complications of multiple beam transport within its large diameter induction core structure. The rf linacs accelerate single beams in smaller (but still large) resonant structures.

Table 1

Heavy Ion Linacs Leading to a Fusion Driver

Name	Role	Ion	Kinetic Energy	Number of Beams	Total Energy
SBTE	Quadrupole Transport of Space Charge Dominated Ion Beams	Cs^+	150 kV	1	--
MBE	Longitudinal and Transverse Dynamics with Multiple Beams	Cs^+	200 MeV $\rightarrow$ 1.0 MeV	4	.08 J
ILSE - Proposed 1989	Beam Dynamics, esp. with Magnetic Quadrupoles and Bends	C^+	2.0 MeV $\rightarrow$ 10.0 MeV	16 $\rightarrow$ 4 $\rightarrow$ 1	60 J
Intermediate Facility - 1990 Concept	High Current Dynamics, Component Development and Integration	K^+	100 MeV	84 $\rightarrow$ 21	30 kJ
LMF	Defense Applications and Power Driver Development	Kr^+	2.5 GeV	24	5.0 MJ
Power Driver - 1990 Concept	Prototype	Hg^+	10.0 GeV	20 $\rightarrow$ 4	4.0 MJ

(4) The rf system has many stations involving delicate beam manipulations, that can result in a serious loss of particles and beam quality. The induction linac must have very accurate control of acccelerating pulse forms to control beam quality.

(5) Issues of beam stability arise for the storage rings in the rf approach and for the interaction of the beam with induction modules in the induction linac. Both appear solvable at present, but at some expense.

(6) Residence time of beam in the rf system is one to two orders of magnitude longer than in the induction linac. This places a much more severe vacuum requirement of the rf system.

(7) The two systems are essentially the same in final compression and final focus.

As mentioned, an LMF driver can differ from a power plant driver in repetition rate and efficiency. This allows some cost reduction features, which are exploited in the present design:

1) Small standoff distance of final focus lenses from fusion target reduces the size of final focus system and relaxes some beam requirements.

2) A vacuum environment in the target chamber may eliminate the need for high speed shutters and rapid vacuum pumping at the chamber interface.

3) Pulsed, n-rmal (Cu wire) magnets may be used instead of superconductors due to low pulse rate. However, a moderate pulse rate (~.1 Hz) will be valuable for preshot tuning.

4) Pulsed power components such as capacitors and high power switches can be rated for ~ 10^6 - 10^8 shots instead of ~10^{10} as in a power driver.

The heavy ion driver program in the USA has concentrated on resolving <u>beam dynamics issues</u> for the 15 years of its existence. These have included studies of high current transport, beam compression, stability, high current source operation, multiple beam acceleration, electrostatic aberrations and other driver-related features. Scaled down machines and experiments have demonstrated much of the fundamental accelerator physics and technology. Some areas of beam dynamics such as high current effects in magnetic quadrupole transport, bends and final focus have not been explored and are a subject of the near-term research program (ILSE). Most development needs have been unaddressed due to a lack of resources and no account of these is given here. However, all stages of the driver system employ large, high power versions of the components used in the present beam dynamics study program and can be assumed to require prototype development before an LMF or power driver can be realistically designed.

4. Beam Requirements and Tradeoffs

ICF requires very high power and total energy deposited on the fusion target, roughly independent of driver type. However, unlike lasers, conversion efficiency to x-rays is thought to improve with increased driver energy, and focal spot sizes can be larger by a factor of several. For an ion driver the depth of deposition in a stopper must be small ($\lesssim .1$ gm/cm^2) to produce high gains. This range condition can be met in principle by any ion species accelerated sufficiently to match the range-energy relation (see Fig. 2). The very large stopping power for heavy ions in matter allows the use of kinetic energies up to 20 GeV. Required particle currents are therefore low compared with those for photons or light ions, but they are also very high compared with those usually associated with heavy ion accelerators.

The target gain and peak power curves published by Bangerter and Ho[14] are adopted as the starting point of design (Figs. 3,4). Here the target is indirectly driven with double sided illumination. The clusters of ion beams heat a stopping material by classical deposition, and the typical range-energy curves computed [15] for hot Aluminum (200 eV and .2 gm/cm^3 in Fig. 2) are assumed to be adequate for concept definition. After some design iterations, a consistent beam parameter set at the target was selected (Table 2).

Although essentially similar, heavy ion-driven targets differ from laser-driven targets due to the different mode of energy disposition (Figure 5). They resemble light ion targets in this respect, but generally have a much smaller area of energy deposition. Thus, although much information about target performance may be inferred from the laser and light ion experimental programs, heavy ion targets will be primarily studied by computer simulation for the forseeable future (as in reference 14). Data about range vs. energy and range shortening in hot dense plasmas, and other relevant plasma properties are expected from the European program on a time scale of several years. This may be used for code validation.

Table 2. Beam Parameters at the Target

Gain	(G)	90
Beam Energy	(W)	5 MJ
Target Yield	(Y)	450 MJ
Range	(R)	.1 gm/cm^2
Spot Radius	(r)	2.0 mm
Ion Mass (Kr^+)	(A)	83.9 amu
Peak Power	(P)	480 TW
Kinetic Energy	(T)	2.5 GeV

Twenty five percent of the 5 MJ beam energy is used for a prepulse (picket fence), so effective pulse length and peak (total) electric current are

$$\tau_c = .75 \text{ W/P} = 7.81 \text{ ns} ,$$

$$I = P/(T/e) = 192 \text{ kA} .$$

This current is too large to focus and transport directly to the target in two beams; it must be subdivided into many beams. A total of 24 individual beams are employed, with 18 in the peak power pulse and 6 arriving early to make up a prepulse. The peak current of an individual beam is then $I_p = 192/18 = 10.67$ kA. At this level a 91% charge-neutralization fraction (in the chamber) must be supplied by co-injected electrons to allow the 2 mm focal spot.

Several significant design tradeoffs are apparent,and the selected working point represents a balance among these. First, it is clear that reduced spot radius increases gain if all other parameters are fixed; this would allow the use of a lower total energy for a fixed yield. However, reduced spot size significantly increases technical risk in final focus and chamber transport. A more subtle scaling with smaller spot size is that the beams must occupy a smaller 6-d phase space during acceleration, which tightens tolerances on beam control and restricts ion sources and possibly reduces transportable current. Reduced range in the stopper also increases yield. This can be accomplished by either increasing ion mass or reducing kinetic energy. Ion mass has already been assumed very large for heavy ion drivers in order to get short ranges, and the switch to Kr^+ from the often assumed Hg^{+++} is motivated by the present day absence of a suitable, long pulse, high current source for the latter ion. Ion kinetic energy is reduced from ~ 9 GeV to 2.5 GeV when we adopt Kr^+ in order to hold range at ~.1 gm/cm^2. The similar values of charge to mass ratio and total accelerating voltage for these two ions insures that the drivers would be similar in size and cost. A further reduction in ion energy below 2.5 GeV would raise total driver cost due to the resulting low accelerating gradient at the low energy end and increased number of beams at the chamber associated with the increased total beam charge.

In summary, a broad optimum of driver cost is thought to exist around 2.5 GeV Kr^+ or 9 GeV Hg^{+++}. The latter ion would have a small advantage in cost if a source existed. For either ion a fairly high degree of charge neutralization is required in the chamber, and this is a technical issue which is assumed to be favorably resolved here. The alternative of 9.0 GeV Hg^+ ions would not require neutralization, but would require an appreciably longer and more expensive linac. A second, more expensive, solution to the space charge problem is to use a larger number of beams in final focus (preceded by a beam splitting operation).

5. Chamber

No study of chamber stress has been made for a heavy ion LMF. It is simply assumed here that a protected first wall at 2.0 m radius will be adequate (compare e.g., the 1.5 m first wall radius of a light-ion LMF). A 1.0 m thick layer for radiological shielding follows, which is penetrated by 24 beam ports of about 15 cm maximum diameter each. These ports are located in two clusters of 12 each on opposite sides of the chamber, with a maximum width between beam axes of 25° (see Fig. 6). The edge of the nearest final focus magnet is conservatively located at about 3.25 m radius to avoid heating of the insulated wire by neutrons. Neutralizing electron beams are co-injected parallel to the ions from grid sets located at about 2.75 m radius. These grids may be sacrificial. The concentration of beams into two groups of only moderate angular spread is a significant advantage of the heavy ion driver for the LMF application. If additional space is required around the fusion target, the chamber could be designed with a radius larger than the assumed 2.0 m. The last final focus magnets would stay at 3.25 m radius, but would be protected by a shield intruding into a chamber. Equivalently, in Figure 6 the chamber would bulge outwards in the plane normal to the beam groups.

The chamber is assumed to operate below 10^{-6} torr (N_2 or equivalent) vacuum, so that final focus can be differentially pumped without difficulty to 10^{-7} torr. Stripping of beam ions in final focus is then held to a very low level and the co-injected electrons follow the beams without scattering. Although the low pulse rate allows vacuum operating conditions, it is necessary to include fast shutters in the final focus beam lines to restrict radioactive vapors to a small portion of the driver system.

Line-of-sight neutrons in the beam ports do not intersect insulated magnet cable until the third quadrupole is reached at ~ 15 m radius. If necessary, by using quadrupoles with noncylindrical aperture, line-of-sight neutrons can be dumped in absorbers located between magnets for the entire final focus system.

The chamber must be equipped with vacuum seal doors for access, diagnostics, and beam ports.

6. Beam Quality

Beam spot radius is determined by at least five factors: transverse phase space area, space charge, second order chromatic aberration in final focus, third order geometric aberration in final focus, and jitter of all types. All are strongly dependent on the beam convergence half angle (θ). The aberrations are reduced by small θ, and the other effects are reduced by large θ. Here we set $\theta = 20$ mr, at which value geometric aberration can be essentially eliminated by design in final focus. The other four sources of spot size are taken to contribute equally in the square, i.e. each individually would produce a spot radius $\tilde{r} \equiv (r^2/4)^{1/2} = 1.0$ mm.

Taking $\tilde{r}$ to be an upper bound for radius produced by transverse phase space area, we have the limit on beam emittance (normalized edge value)

$$\varepsilon_n \leq \beta\theta\tilde{r} \leq 5.06 \times 10^{-6} \text{ m-r},$$

where

$$\beta = \frac{v}{c} = .253 \text{ for } 2.5 \text{ GeV } K_r^+ \quad .$$

(non-relativistic formulas are used in this study.)

Momentum spread, assuming a four quadrupole final focus system with focal length/magnet $F = 4.0$ m, is approximately bounded by

$$\frac{\Delta p}{p} \leq \pm \frac{\tilde{r}}{8F\theta} = \pm\ 1.56\times10^{-3}.$$

This assumes that no second order optical correction scheme is used.

Space charge neutralization fraction (*f*) is

$$f \geq 1 - \frac{\theta^2}{2\kappa \ell n(F\theta/\tilde{r})} = .912 \ ,$$

where κ is the dimensionless perveance of the focussed beam in the chamber:

$$\kappa = \frac{2eI}{\beta^3 Mc^3 4\pi\varepsilon_o} = 5.16\times10^{-4} \ ,$$

and I is taken to be 2% larger than the peak value in the target spot.

7. Summary of Major Parameters

The major parameters of the LMF at or near the target are summarized in Table 3.

Table 3

Summary of Major Parameters

Target Type		Indirect drive double-sided illumination
Target Yield	(Y)	450 MJ
Beam Energy on Target	(W)	5.00 MJ
Peak Power on Target	(P)	480 TW
Beam Spot Radius	(r)	2.00 mm
Ion Range	(R)	.100 gm/cm^2
Target Gain	(G)	90.0
Prepulse Energy Fraction		25%
Number of Beams	(N)	24
Ion Type		Kr^+
Ion Mass	(A)	83.91 amu
Ion Charge State	(q)	+ 1
Ion Kinetic Energy	(T)	2.50 GeV
Effective Pulse Length	(τ_e)	7.81 ns
Total Charge on Target Spots		2000 μC
Beam Emittance	(ε_n)	$< 5.06 \times 10^{-6}$ m-r
Beam Convergence Half Angle	(θ)	20.0 mr
12 Beam Group Angular Spread		± 12.5°
Particle Velocity	($\beta = v/c$)	.253
Particle Rigidity	(Non-relativistic $B\rho$)	65.9 T-m
Peak Current Per Beam in Spot	(I_p)	10660 Amp
Radius of First Wall		2.00 m
Standoff to First Magnet		3.25 m
Chamber Gas Pressure (N_2 at 20°C)		$< 10^{-6}$ torr
Momentum Spread	$\Delta p/p$	$< \pm 1.56 \times 10^{-3}$
Beam Neutralization Fraction by co-injected electrons	(f)	> 91.2%

B. HEAVY ION DRIVER SYSTEM

1. General Features of an Induction Linac System for ICF (Power Production or LMF)

An induction linac driver for ICF is now envisioned as a multiple-beam transport lattice consisting of N closely packed, parallel FODO transport channels. Each focusing channel is composed of a periodic system of focusing (F) and defocusing (D) quadrupole lenses with acceleration gaps (O) between successive lenses. Surrounding the transport structure are large induction cores of ferromagnetic material with associated pulser circuitry that apply a succession of long-duration, high-voltage pulses to the N parallel beams as they jointly pass through acceleration gaps. Longitudinal focusing is achieved through the detailed timing and shape of the accelerating waveforms (with feedforward correction of errors). A multiple-beam source of heavy ions operates at about 2 MV, producing the net charge per pulse required to achieve the desired pellet gain. Initial current and, therefore, initial pulse length are determined by transport limits at low energy, which are in turn proportional to injector voltage. ICF power driver designs often employ a large number of electrostatic quadrupole channels (N = 32 - 128) at low energies (below ~ 100 MeV), followed by a lower number of superconducting magnetic channels (N~4-32) for the rest of the accelerator. Merging of beams would therefore be required at the transition and some splitting of beams at final energy might be required to stay within current limits in final focus. A conceptually simpler, lower risk design with possibly higher cost makes use of magnetic quadrupoles for the entire system without combining or splitting. For a power driver these would be superconducting in order to achieve reasonable electrical efficiency. For the LMF design presented here we adopt the lower risk approach, with N = 24 beams for the entire system. Pulsed magnets using copper wire may be employed since the repetition rate is very low. The use of pulsed, current dominated magnets (without iron poles) also allows field strengths approaching those attainable with superconducting wire.

The reason for the use of multiple beams is that it increases the net current that can be accelerated within a given cross section of core at a fixed accelerating gradient. Alternatively, a given amount of charge can be accelerated more rapidly with multiple beams since the pulse length is shortened and a core cross section of specified volt-seconds per meter flux-swing can supply an increased gradient. However, an increase in the number of beams of given current increases the dimensions and cost of the transport lattice and also increases the cost of the core for a given volt-second product since a larger core volume is required. For a core of given cross sectional area (proportional to volt-seconds per meter), the volume of ferromagnetic material increases as its inside diameter is increased. Hence, there is a trade-off between transport and acceleration costs with an optimum at some finite number of beams. The determination of this optimum configuration is a complex problem depending on projected costs of magnets, core, insulators, energy storage, pulsers, and fabrication. However computer codes for optimizing a power driver exist and could be modified for LMF purposes.

Induction cores (Fig. 7) are most likely to be constructed from very thin laminations of amorphous iron, which is the preferred material due to its excellent electrical characteristics and flux-swing. At a projected future cost of approximately \$5.0/kg for insulated and wound tape, this is a major cost item for the first 1 to 2 GV of a typical linac. Here it is assumed that a cheap insulator can be developed for tape available at ~3.30 \$/kg. At higher cumulative voltage, the cost of pulsers and fabrication of the high gradient column with vacuum insulators dominates cost projections for the induction module.

Between the accelerator and the fusion chamber, the beams are separated radially in space. The N drift lines leading to the final focus area are 100 to 600 m long and used for ballistic compression as well as to match the final focus configuration into the chamber. This transport lattice is composed of high-field quadrupoles, bends, and possibly higher-order focal elements needed to control momentum dispersion and aberrations. As the beams compress, the transport of the high current becomes increasingly demanding, with the large apertures and the close packing of quadrupoles especially pronounced immediately before the final focus area.

The final focus system itself has parameters determined largely by the requirements of spot size, target chamber size, beam rigidity (rigidity = momentum/charge = $|B\rho|$), and the handling of neutrons, x-rays, and gas flux from the chamber. The final focus magnet train is composed of four (or more) magnetic quadrupoles of large bore. With four quadrupoles its total length is approximately five times the focal length of an individual magnet.

2. Pulse Structure

Beam pulse length decreases dramatically between the injector operating at 2 MeV and final focus at 2.5 GeV. Current increases accordingly, due both to acceleration and spatial compression. For the entire system the current profile is assumed to have a flat top, with rise and fall times equal to 1/11 of total pulse duration (τ). Therefore the flat top is 9/11 of the total and the effective pulse length (τ_c = charge/peak current) is 10/11 of the total. It is expected that some beam loss will occur through the system; to include this feature in the model, the loss is taken to be 2% at each major transition point. Pulse parameters for major components are given in Table 4.

Table 4

Beam Pulse Parameters for Major LMF Components

Component	Total Pulse Charge (μC)	Cumulative Voltage (MV)	Total Beam Pulse Length	Peak Current Per Beam
Source/Injector	2213	0.0 → 2.0	45.9 μs	2.21 A
Matching Section	2213	2.0	45.9 μs	2.21 A
Linac: Low V Section	2168	2.0 → 25.6	45.9 → 3.58 μs	2.17 → 27.8 A
Linac: Medium V Section	2168	25.6 → 91.7	3.58 → 1.0 μs	27.8 → 99.4 A
Linac: High V Section	2168	91.7→ 2500	1.0 → .132 μs	99.4 → 753 A
Drift Compression	2125	2500	132 ns → 8.59 ns	.737 → 11.3 kA
Final Focus	2082	2500	8.59 ns	11.1 kA
Chamber (Neutralized)	2041	2500	8.59 ns	1.09 A
Target	2000	2500 → 0.0	8.59 ns	1.07 kA

Total pulse charge takes into account a 2% loss at five locations. Peak current is 1.1 times mean current per beam (= total charge/24 x total pulse length).

3. Injector

Twenty four beams of 2.0 MeV Kr^+ are supplied by a source/injector system, with peak current per beam of 2.21 amperes and total pulse length of 45.9 μs. Voltage control must be excellent (< ±1.0%) to maintain sufficiently low occupied longitudinal phase space area. The source is a large area, gas discharge with ions exiting a highly perforated cathode held about 100 kV below the +2 MV discharge volume. Sources of this type are an extrapolation from the long pulse type developed for neutral beam heating of magnetic fusion devices and are currently being developed at LBL for ILSE. They are also similar to the large aperture Cs^+ and Hg^+ sources developed for application as ion thrusters. The remaining ~1.9 MV of the injector is a high gradient column, with aperture focussing provided by voltage grading corresponding approximately to the Child-Langmuir Law (i.e. $V(x) \propto x^{4/3}$).

An estimate of injector parameters is readily made. Taking the maximum injector gradient be 5 MV/m we find column length

$$d = \frac{4}{3}\frac{V}{\varepsilon_{max}} = .533 \text{ m} .$$

By applying the C-L current density law

$$j = 5.46\times10^{-8}\sqrt{\frac{qV^3}{Ad^4}} = 59.4 \text{ A/m}^2 ,$$

we obtain the beam radius

$$a_s = \sqrt{\frac{I}{\pi j}} = .109 \text{ m} .$$

This radius is approximately double that desired for a beam in the induction linac, so a bending and matching system with bends must connect the injector to the accelerator. This would require about 5 quadrupoles and 2 bends per beam. The source discharge is expected to produce very low temperature ions (< .5 eV). Assuming an effective value $T_s \leq 1$ eV, which includes injector aberrations, we find initial emittance

$$\varepsilon_n = 6.55\times10^{-5} \sqrt{\frac{T_s}{A}}\, a_s \leq 7.79\times10^{-7} \text{ m-r},$$

a value 6.5 times smaller than the design limit for final focus. Elimination of mechanisms causing emittance growth through the entire driver is therefore crucial.

In order to make an injector system of manageable dimensions, the 24 beams are produced in four groups of six each. Each group of 6 would have a high voltage power supply in common, possibly employing large, amorphous iron blocking cores similar to those of the linac.

4. Beam Transport

The multiple-beam quadrupoles that transport the heavy ions through the linac are built up of Cu cable wrapped close to the beam channels and backed by non-magnetic steel collars. High fields (B ~ 5T) can be realized in this configuration by operating with short pulses, with enough time interval between them for cooling to ambient. In the present design, a maximum temperature rise of 20°C is produced in 5 ms operation with 6×10^8 Amperes/m^2 average in the insulated cable. Peak field at the wire is ~ 3.8 T, producing an average radial force of about 5000 psi on the collar.

All magnets are identical in their transverse dimensions, but their lengths increase by a factor of several over the first 92 MV of the linac. Specific beam and magnet parameters at the lowest energy are given in Table 5.

Approximate relations for quadrupole transport of intense non-relativistic ion beams were used to construct Table 5; these are summarized in an Appendix on pg. 33.

Table 5
Transport Parameters at 2 MV

Ion Mass (Kr^+)	(A)	83.9 amu
Kinetic Energy	(eV_0)	2 MeV
Peak Beam Current	(I)	2.17 A
Beam Edge Radius	(a)	5.67 cm
Transport Tune	(σ_0)	72°
Depressed Tune	(σ)	2.5°
Velocity/c	($\beta = v/c$)	.00715
Rigidity	[$B\rho$]	1.86 T-m
Magnet Aperture	(R)	8.09 cm
Wire Inner Radius		9.09 cm
Wire Outer Radius		10.0 cm
Field Gradient	(B')	38.2 T/m
Lattice Half Period Length	(L)	38.2 cm
Magnet Effective Field Length	(ηL)	18.2 cm

The phase advance per period (tune σ_0) of 72° is selected to ensure that the entire pulse is free from an envelope instability associated with $\sigma_0 > 85°$. The depressed tune of 2.5° is consistent with the source emittance. A significant feature of the magnets is their large aspect ratio $R/\eta L = .445$ at the lowest energy. Special design consideration is necessary to minimize aberrations at this stage, but there is little problem with this for most of the machine.

Beam space charge nearby cancels the focussing action of the quadrupoles. This is a consequence of the relatively large value of the current for the required emittance, and is reflected in the very low ratio of depressed tune to transport tune [$\sigma/\sigma_0 \propto \varepsilon_n V \sigma_0 /LI$] .Experimental demonstration[9] of transport using electrostatic quadrupoles (SBTE) has shown stability down to

$\sigma/\sigma_0 \approx .1$, limited only by available source emittance. The lower ratio $\sigma/\sigma_0 \approx .035$ assumed here is expected to be stable for magnetic transport, based on PIC simulations.[16]

Magnet length increases during acceleration at a rate which balances space charge forces while maintaining constant beam radius and magnetic field gradient. The essential scale relations for quadrupole occupancy (η) and half period length (L) are approximately

$$\eta L^2 V^{-1/2} = \text{constant},$$

$$I L^2 V^{-3/2} = \text{constant},$$

where I is peak beam current and V is cumulative accelerating voltage.

In the low and medium energy linac sections ($V < V_2 = 91.7$ MV) we have

$$\eta = .476,$$

$$L = .382\,(V/V_0)^{1/4}\ \text{m},$$

so at V_2, L = .994 m and the effective magnet length is ηL = .473 m. For the high energy section ηL is the constant value .473 m, while η decreases gradually to .110 and L increases to 4.30 m.

5. Acceleration Section Parameters

5.1 Low energy section ($V_0 = 2\text{ MV} < V < 25.6\text{ MV} = V_1$)

The rate of acceleration at the lowest energy is limited by beam dynamics; in order to avoid a degradation of transport, the pulse tail is not allowed to have velocity significantly larger than the pulse head. The assumed requirement is $\Delta v/v \leq .3$ at any station in the accelerator, where $\Delta v = (v_{tail} - v_{head})$ and $v = (v_{tail} + v_{head})/2$. The "velocity tilt" $\Delta v/v$ is the consequence of both acceleration and longitudinal compression. A useful relation is

$$\frac{\Delta v}{v} = \frac{\varepsilon \ell}{V}\left[\frac{1}{2} - \frac{d\ell n(\ell)}{d\ell n(V)}\right] ,$$

where ε is the smoothed, local system gradient, $\ell = v\tau$ is pulse length given in meters, and V is cumulative voltage. In the low energy section compression and acceleration are taken to contribute equally to tilt ($\ell \propto V^{-1/2}$). We find at $V_0 = 2$ MV:

$$\tau_0 = 45.9\ \mu s \text{ (total pulse durations are given)} ,$$

$$\varepsilon_0 = 6.10\ \text{kV/m} ,$$

$$\ell_0 = 98.4\ \text{m} ,$$

$$\varepsilon_0\tau_0 = .280\ \text{V-s/m} ,$$

and for $V_0 < V < V_1 = 25.6$ MV the scaling with V is

$$\tau = \tau_0\, V_0/V ,$$

$$\ell = \ell_0\, (V_0/V)^{1/2} ,$$

$$\varepsilon = \varepsilon_0 (V/V_0)^{3/2} ,$$

$$\varepsilon\tau = \varepsilon_0\tau_0\, (V/V_0)^{1/2} .$$

Acceleration in this manner continues to V_1, where the volt-sec product reaches 1.0 V-s/m. At this point we have

$$\tau_1 = 3.58\ \mu s ,$$

$$\ell_1 = 27.5\ \text{m} ,$$

$$\varepsilon_1 = 279\ \text{kV/m} .$$

Total section length, volt sec product, and number of lattice half periods are readily obtained for $V_o < V < V_1$:

$$\text{Low energy section length} = \int \frac{dV}{\varepsilon} = 472\ \text{m}\ ,$$

$$\text{Volt-sec total} = \int \frac{dV}{\varepsilon}\,\varepsilon\tau = 234\ \text{V-s}\ ,$$

$$\text{Half periods} = \int \frac{dV}{\varepsilon L} = 373\ .$$

5.2 Medium energy section ($V_1 = 25.6$ MV $< V < V_2 = 91.7$ MV)

Here acceleration is limited by core size -- we restrict $\varepsilon\tau$ to be 1.0 V-s/m (the total flux swing per m is ~20% larger than this value). Compression as $\ell \propto V^{-1/2}$ continues, so the scale relations are

$$\frac{\Delta v}{v} = .3(V_1/V)^{1/2}\ ,$$

$$\tau = \tau_1\,(V_1/V)\ ,$$

$$\varepsilon = \varepsilon_1(V/V_1)\ .$$

This schedule applies up to $V_2 = 91.7$ MV, where gradient $\varepsilon_2 = 1.0$ MV/m is reached. We then have

$$(\Delta v/v)_2 = .158\ ,$$

$$\tau_2 = 1.0\ \mu\text{s}\ ,$$

$$\ell_2 = 14.5\ \text{m}\ .$$

Summary for medium energy section:

Medium energy section length = 117 m ,

Section core = 117 Volt-sec ,

Section half periods = 139 .

5.3 High energy section ($V_2 = 91.7$ MV < V < 2.5 GV = V_3)

Acceleration gradient ε is now limited by the breakdown field of vacuum insulators for finite duration pulses. A conservative relation between mean gradient and pulse length is achieved with

$$\varepsilon = \varepsilon_2 (V/V_2)^{1/4} .$$

Pulse compression continues to a minor degree, but is brought to a halt at ℓ = 10.0 m to keep the longitudinal space charge fields within manageable bounds. While there is no physical limit here it would be inconvenient to devote major resources to keeping a short bunch together. To achieve a smooth transition at V_2 and satisfy the gradient and pulse length conditions in the high energy section we take

$$\ell = \ell_2 \left[1 + \frac{\sqrt{V/V_2} - 1}{1 + 1.97(\sqrt{V/V_2} - 1)} \right]^{-1} ,$$

$$\tau = \tau_2 \sqrt{\frac{V_2}{V}} \frac{\ell}{\ell_2} .$$

Then as V reaches the final value 2.5 GV we have the final values

$$\varepsilon_3 = 2.28 \text{ MV/m} ,$$

$$\tau_3 = .132 \ \mu\text{s} ,$$

$$\ell_3 = 10 \text{ m} .$$

The particular formulas given for ℓ and ε guarantee that tilt $\Delta v/v$ is continuous at the 91.7 MV transition point. Summary for high energy section:

High energy section length = 1336 m ,

Section core = 568 Volt-sec. ,

Section lattice periods = 521.

Total length, core and half periods for the entire linac are:

Length = 1925 m ,

Core = 919 Volt-sec. ,

Half periods = 1033 .

6. Drift-Compression

A large amplification of beam power is possible subsequent to acceleration. The beam pulse length is reduced by a factor of ~15.3 between the linac and final focus by drift-compression. During the final stages of acceleration a large velocity tilt is re-imposed for this purpose through the use of ramped waveforms in the induction modules (this is not included in the calculations of Sec. 5.3). Longitudinal space charge force removes this tilt by the time the beam reaches final focus. The consistent parameter set in this design is: drift distance to middle of final focus system = 159 m , initial tilt $\Delta v/v = .0667$, assuming the space charge weight factor is $g = 2\ell n(R/\bar{a}) = .81$. Transport into the final focus configuration requires bends up to 4.0 T field strength (well below the ~6.7 T of SSC) and quadrupoles of increased aperture. A 50 m mean radius of curvature is adequate for the bend system; thus bend occupancy fraction is the moderate value

$$\eta_{bend} = \frac{\text{ion rigidity}}{\text{B x mean radius}} = \frac{65.9}{4 \times 50} = .330 \quad .$$

In order to transport the increasing current, half period length is gradually decreased by a factor of $\sqrt{3}$ to 2.48 m, and aperture radius increased by $\sqrt{5.1}$. Then $I \propto (R/L)^2$ allows transport of the increased current by the desired factor of 15.3. Quadrupole occupancy fraction increases from an initial value $\eta = .110$ to a final $\eta = .365$, holding gradient $B' = 39.5$ T/m. Magnetic field at the wire rises to ~ 8.5 T, indicating the use superconductor for at least this portion of the system. A detailed layout of this section would include additional magnets needed to maintain first, and possibly second order, achromaticity.

7. Final Focus

Four large-aperture quadrupoles per beam are adequate for a final focus set. These are laid out as shown in Fig. 8. The focal length (F) is 4.0 m for all. Vertical and horizontal beam envelope radii are also shown in Fig. 8 as calculated using the thin lens approximation. Note that the maximum beam radius is $3F\theta = .24$ m, which occurs in the center pair of quadrupoles; these must be much larger than the others. A point-to-point focus is produced by the layout; this is an adequate approximation for the purpose of obtaining field strengths and sizes. However, a real design would take into account space charge, geometric aberrations, thick lenses, and possibly chromatic corrections. Approximate field strength in each quadrupole is obtained from the thin lens formula

$$B(R_a) = B'R_a = \frac{[B\rho]R_a}{\ell_m F} ,$$

where $[B\rho] = 65.9$ T-m is ion rigidity, R_a is aperture radius, and ℓ_m is effective magnet length. The latter quantity is selected to keep fields as low as possible while allowing room for beam line hardware. Table 6 gives parameter values for large and small final focus quadrupoles

Table 6

Final Focus Parameters

	ℓ_m	R_a	$B(R_a)$
Small Quadrupoles	1.0 m	.14 m	2.31 T
Large Quadrupoles	2.0 m	.28 m	2.31 T

The actual length of a magnet is about 1.5 ℓ_m, and the aperture radii have been set ~17% above the maximum beam radii in the magnets. Field strengths are low enough that pulsed Cu/steel magnets may be used. The full diameter of the large magnets is 1.0 m; this determines the ±12.5° angular spread among beam centers.

7. Concept Validation

Here only a list of requirements will be given; These are separated into the several broad areas:

Dynamics of space charge dominated beams

Special considerations for high power beams

Development of accelerator components

Diagnostics and controls for a large multiple beam induction linac

Cost reduction of accelerator components

Handling high energy ion beams in the experimental area

(1) Dynamics of Space Charge Dominated Beams. This covers stability, emittance growth and general control of beams in which the space charge force nearly cancels the mean focussing effect of the quadrupole channel. The existing experiments, SBTE and MBE, address relevant issues with low current beams (≤ 20 mA) transported over a distance of ~ 20 m. Some acceleration and multiple beam (N = 4) effects have been studied, including current amplification by a factor of 8. The proposed Induction Linac System Experiment (ILSE) will extend this study in several directions, including the use of magnetic quadrupoles, a high voltage injector, bends, drift compression, beam combining and neutralized focus. Low current dynamics should be essentially resolved by ILSE.

(2) High Power Beams. A large currents of ions (> 100 A total) significantly loads the induction modules and thereby acts back on itself. This interaction makes accelerating

waveform control more difficult. In addition, a bunching mode instability is predicted[5]. The resolution of these phenomenon involves developing high resolution waveform and beam current monitors, and high power feed-forward correction circuitry.

A second area of high current effects is the short time-scale degradation of vacuum by beam spill. That is, loss of particles near the beam head can generate an electron cloud which disrupts transport in the beam tail. While this is not as severe an issue for a linac as for a storage ring, it is a significant design issue.

Third, at very high currents the process of neutralization by electrons after final focus may be problematic. For example, it may prove difficult to generate the high currents of electrons with sufficiently low temperature on the nanosecond time scale.

(3) Development of accelerator components. Large induction modules with associated pulser circuitry need to be developed. The goal here is to achieve the desired electrical properties of voltage standoff, impedance and efficiency in a reasonably economical and robust package.

A second area of necessary development is multiple beam quadrupole arrays with adequate field quality and resistance to mechanical and thermal stress.

The 30 kJ intermediate facility appearing on Table 1 would be a useful test bed for categories (2) and (3).

(4) Diagnostics and controls for a large multiple beam induction linac. A driver scale linac requires continual monitoring of beam and magnet positions and a system to make adjustments in alignment. This is more difficult than is usual for accelerators due to the use of multiple beams. Beam steering is also difficult due to the large velocity tilt in the low energy sections.

(5) Cost reduction of accelerator components. At present amorphous iron tape for induction cores is available for ~ 3.30/kg, but an expensive insulating procedure raises the cost by up to an order of magnitude. This price must be drastically reduced to make the induction linac attractive. A second large cost item is the pulser switch and energy storage system. A projected cost of $10/Joule might be realized with special design appropriate for the heavy

ion system, i.e., relatively low rep rate and long pulse compared with existing electron induction linacs.

(6) Handling high energy ion beams in the experimental areas. The heavy ion driver described here employs large magnets and relatively high vacuum close to the target chamber. There are therefore unique interface requirements. These include integration of the neutralization system, fast shutters, space frame and alignment system for magnets, and shielding of activation by the ion beam.

References

1. J. Hovingh et al., Fusion Technology, 13, No. 2, Feb. 1988, 255.

2. Final Report of the Technical Panel on Magnetic Fusion of the Energy Research Advisory Board (DoE Fusion Policy Advisory Committee) September, 1990.

3. M.J. Monsler, The Potential for Reducing the Cost of a Heavy Ion Accelerator for ICF, Satori Technology, Final Report PO#9056305 to LLNL Laser Fusion Program, Feb. 25, 1987.

4. ERDA Summer Study of Heavy Ions for Inertial Fusion, LBL-5543, Dec. 1976.

5. Proceedings of International Heavy Ion Fusion Symposium, Monterey, CA, Dec. 1990.

6. B. Badger et al., HIBALL-II, FPA-84-4, KFK-3840, UWFDM-625, Dec. 1984.

7. T. Godlove, Private Communication.

8. S. Yu et al., HIF Recirculating Induction Accelerator Report in preparation at LLNL.

9. M. G. Tiefenback and D. Keefe, "Measurements of Stability Limits for a Space-Charge-Dominated Ion Beam in a Long A. G. Transport Channel, IEEE Trans. Nucl. Sci, NS-32, 5, 2483, (1985).

10. M. Meuth et al., Nuc. Inst. and Methods in Phys. Res. A278 153, (1989).

11. Induction Linac Systems Experiments - Conceptual Engineering Design Study, LBL PUB-5219, March 1989.

12. C. Fong et al., Intermediate Test Facility and Required Technology Development, May 1990, LBL HIFAR-Note 269.

13. C. Fong, et al., 4 MJ Comparison Driver, LBL HIFAR-Note, Jan. 1991.

14. R. Bangerter and D. Ho, HIFAN-470, Proceedings of the 1990 Linac Conference, September 10-14, 1990, Albuquerque, NM. These results have been adopted for the current DOE/OFE funded study of power generation by inertial fusion.

15. D. Zuckerman et al., Fusion Technology, 13, No. 2, Feb. 1988, 226.

16. I. Haber and C. Celata, Private Communication.

Appendix

Approximate Relations for Intense Beam Transport

$\beta = (2\,T_{MeV}/931.5\,A)^{1/2}$	velocity/c	,
$[B\rho] = 3.107\,\beta\;A/q$	rigidity	,
$K = 30\,I/\beta V$	perveance	,
$a/\bar{a} = 1 + \sqrt{(1 - \cos\sigma_o)/8}$	max/mean edge radii	,
$\cos\sigma_o = 1 - \frac{\eta^2(3-2\eta)}{6}\left(\frac{B'}{[B\rho]}\right)^2 L^4$	phase advance (tune)	,
$\varepsilon_n \cong \beta\sigma\bar{a}^2/2L$	normalized emittance	,
$\cos\sigma - \cos\sigma_o = 2\,K(L/\bar{a})^2$	depressed tune vs. perveance	,

Figure Captions

Fig. 1 Layouts of Heavy Ion Drivers for power plants.

Fig. 2. Range-energy relation for ions in Aluminum (200 eV, .2 gm/cm^2).

Fig. 3. Gain curves for indirectly driven targets giving as a function of driver energy, focal spot radius, and ion range. These curves assume two-sided irradiation.

Fig. 4. Peak power requirements corresponding to the gain curves given in Fig. 3.

Fig. 5 Heavy Ion and Laser-Driven Targets

Fig. 6. Beam geometry

Fig. 7. Induction module

Fig. 8. Final focus layout. Magnet entire lengths, positions and aperture radii are depicted by vertical rectangles. Diagonal lines are the vertical (V) and horizontal (H) beam radii. A simple point-to-point focus is achieved with all focal lengths $F = 4.0$ m.

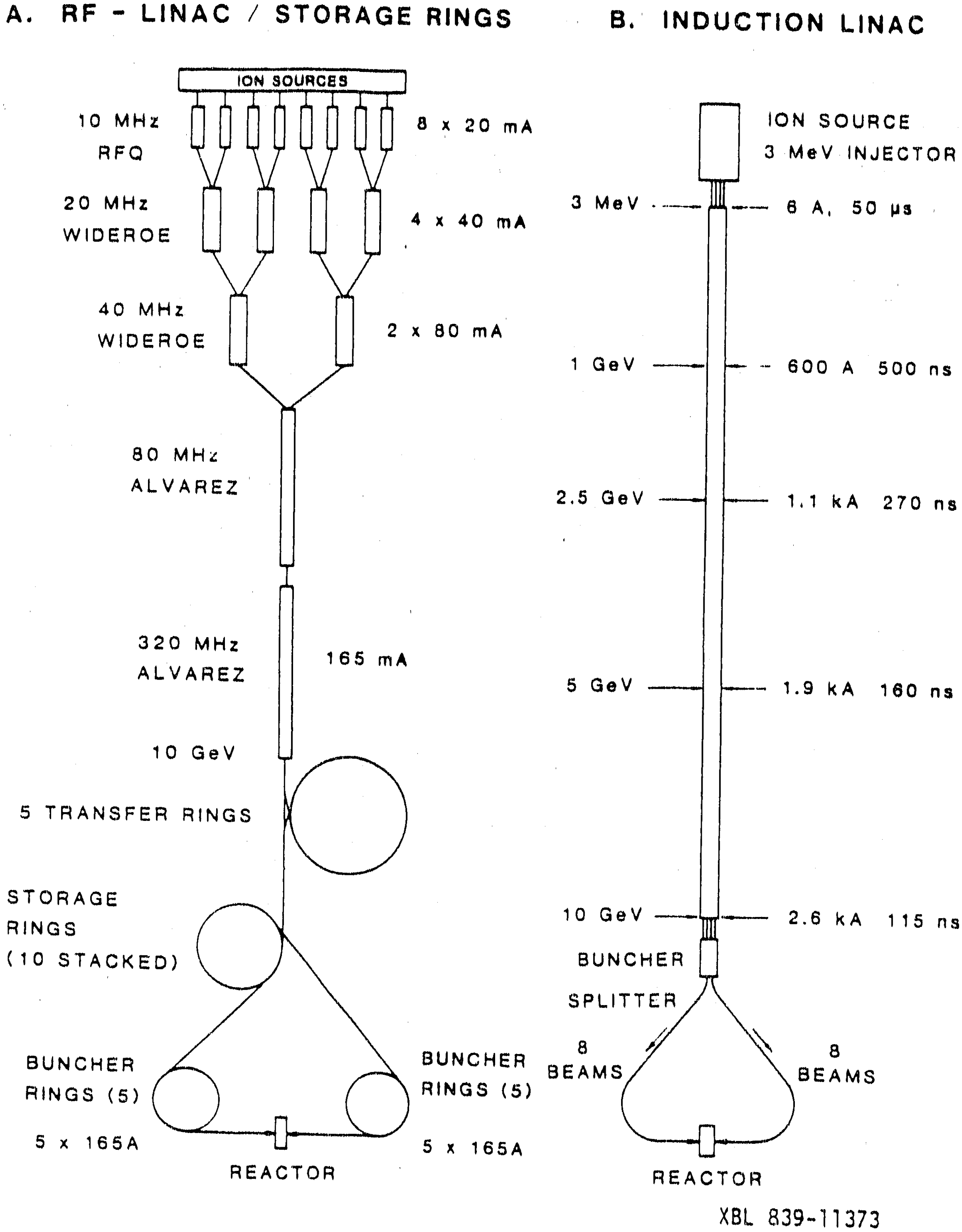
A. RF - LINAC / STORAGE RINGS
B. INDUCTION LINAC
ION SOURCES
10 MHz
RFQ
8 x 20 mA
20 MHz
WIDEROE
4 x 40 mA
40 MHz
WIDEROE
2 x 80 mA
80 MHz
ALVAREZ
320 MHz
ALVAREZ
165 mA
10 GeV
5 TRANSFER RINGS
STORAGE
RINGS
(10 STACKED)
BUNCHER
RINGS (5)
5 x 165A
BUNCHER
RINGS (5)
5 x 165A
REACTOR
ION SOURCE
3 MeV INJECTOR
3 MeV
6 A, 50 μs
1 GeV
600 A 500 ns
2.5 GeV
1.1 kA 270 ns
5 GeV
1.9 kA 160 ns
10 GeV
2.6 kA 115 ns
BUNCHER
SPLITTER
8
BEAMS
8
BEAMS
REACTOR
XBL 839-11373

Figure 1

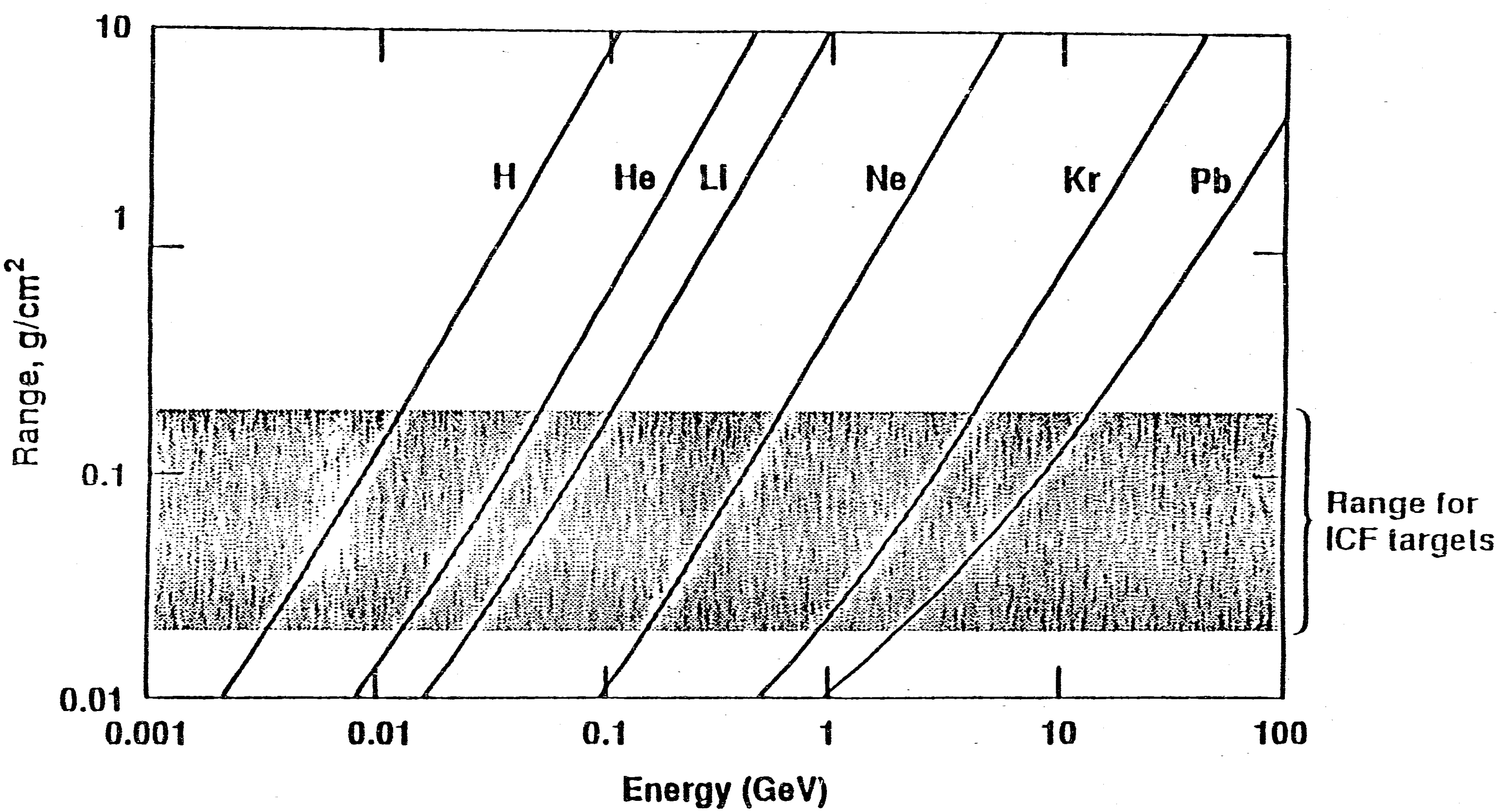
10
1
0.1
0.01
Range, g/cm²
H
He
Li
Ne
Kr
Pb
0.001
0.01
0.1
1
10
100
Energy (GeV)
Range for
ICF targets

Figure 2

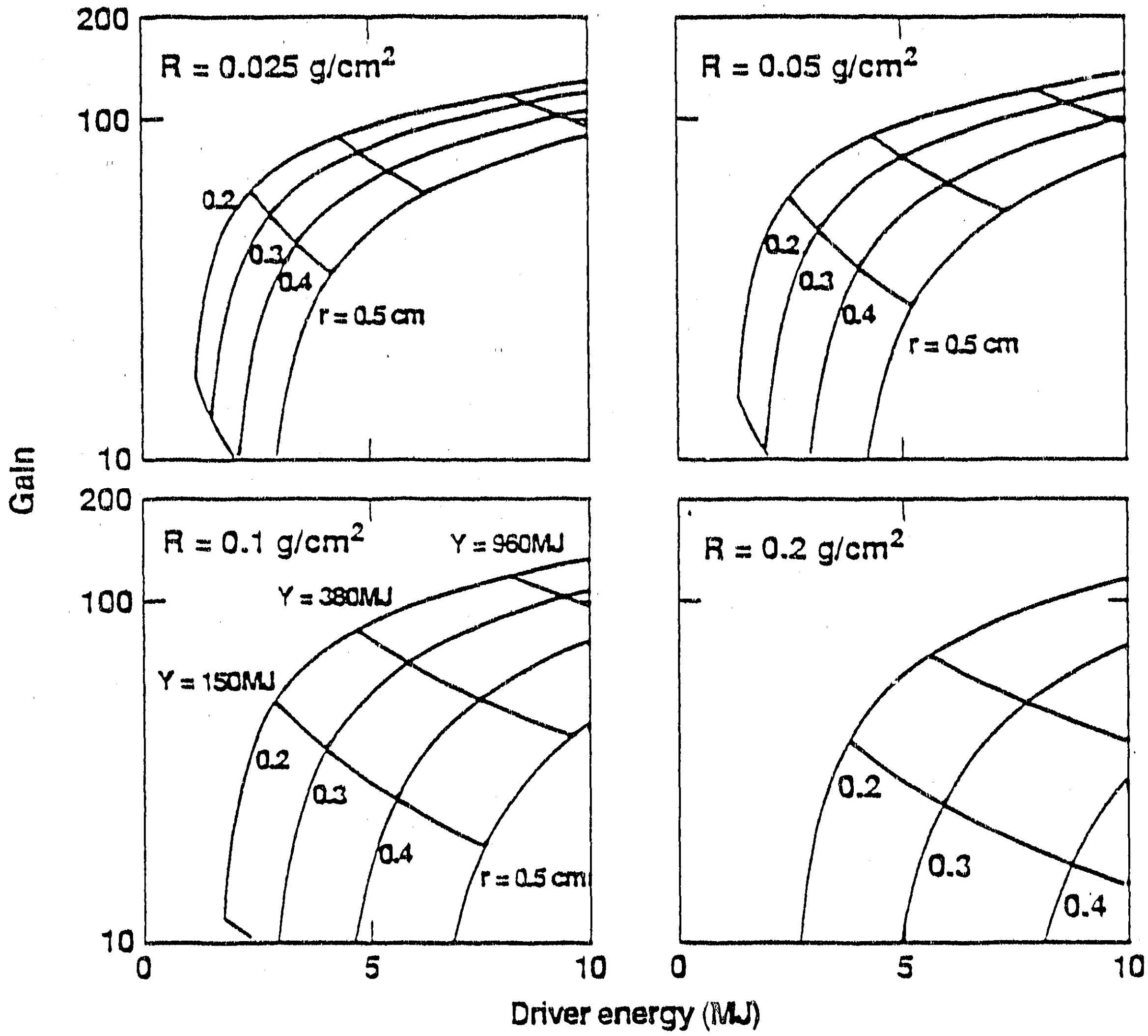
R = 0.025 g/cm²
R = 0.05 g/cm²
R = 0.1 g/cm²
R = 0.2 g/cm²
Y = 960MJ
Y = 380MJ
Y = 150MJ
0.2
0.3
0.4
r = 0.5 cm
Gain
200
100
10
0
5
10
Driver energy (MJ)

Figure 3

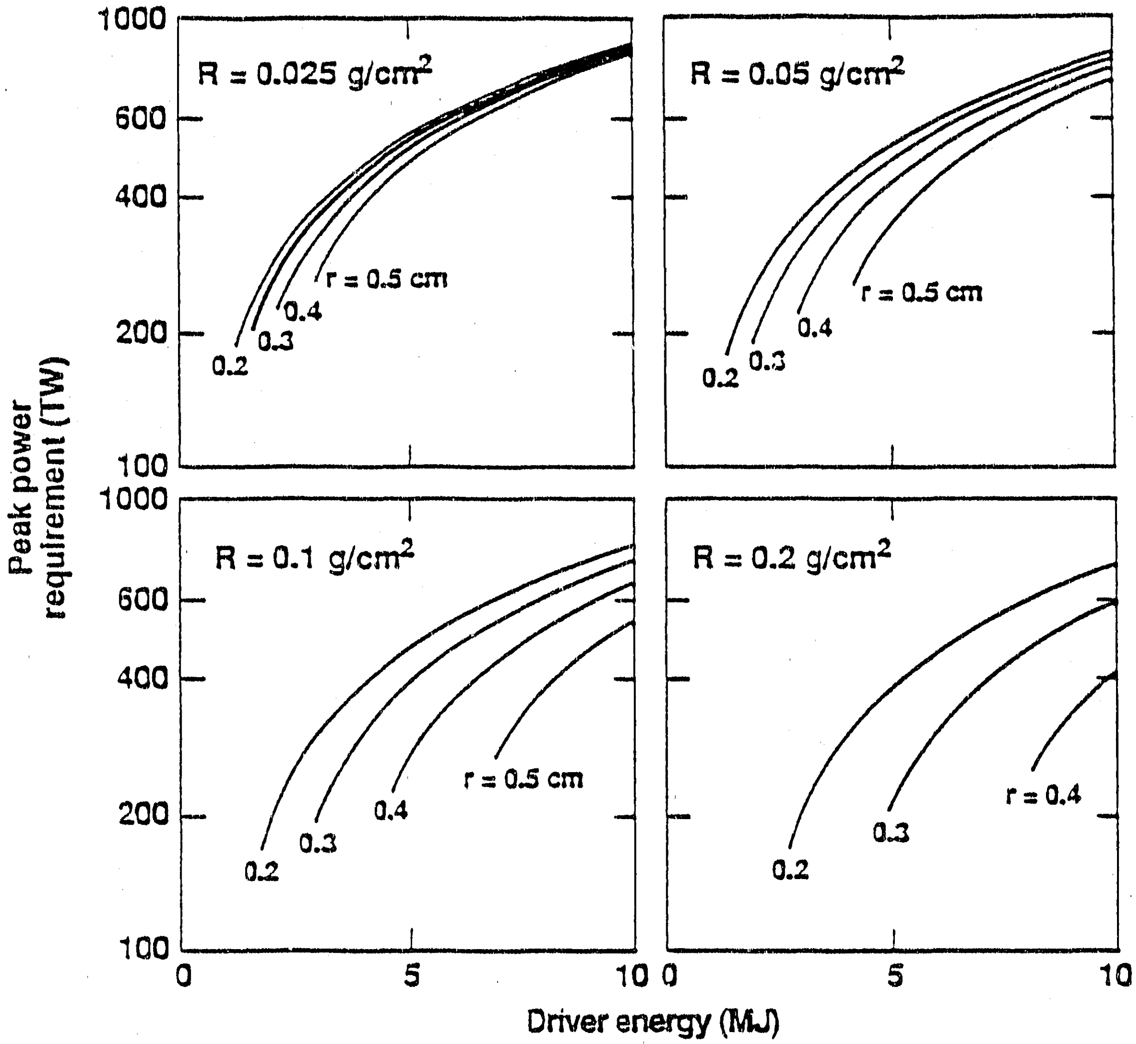

Peak power requirement (TW)
Driver energy (MJ)
R = 0.025 g/cm²
R = 0.05 g/cm²
R = 0.1 g/cm²
R = 0.2 g/cm²
r = 0.5 cm
0.4
0.3
0.2
r = 0.4
1000
600
400
200
100
0
5
10

Figure 4

For indirect drive, capsule physics is essentially driver-independent

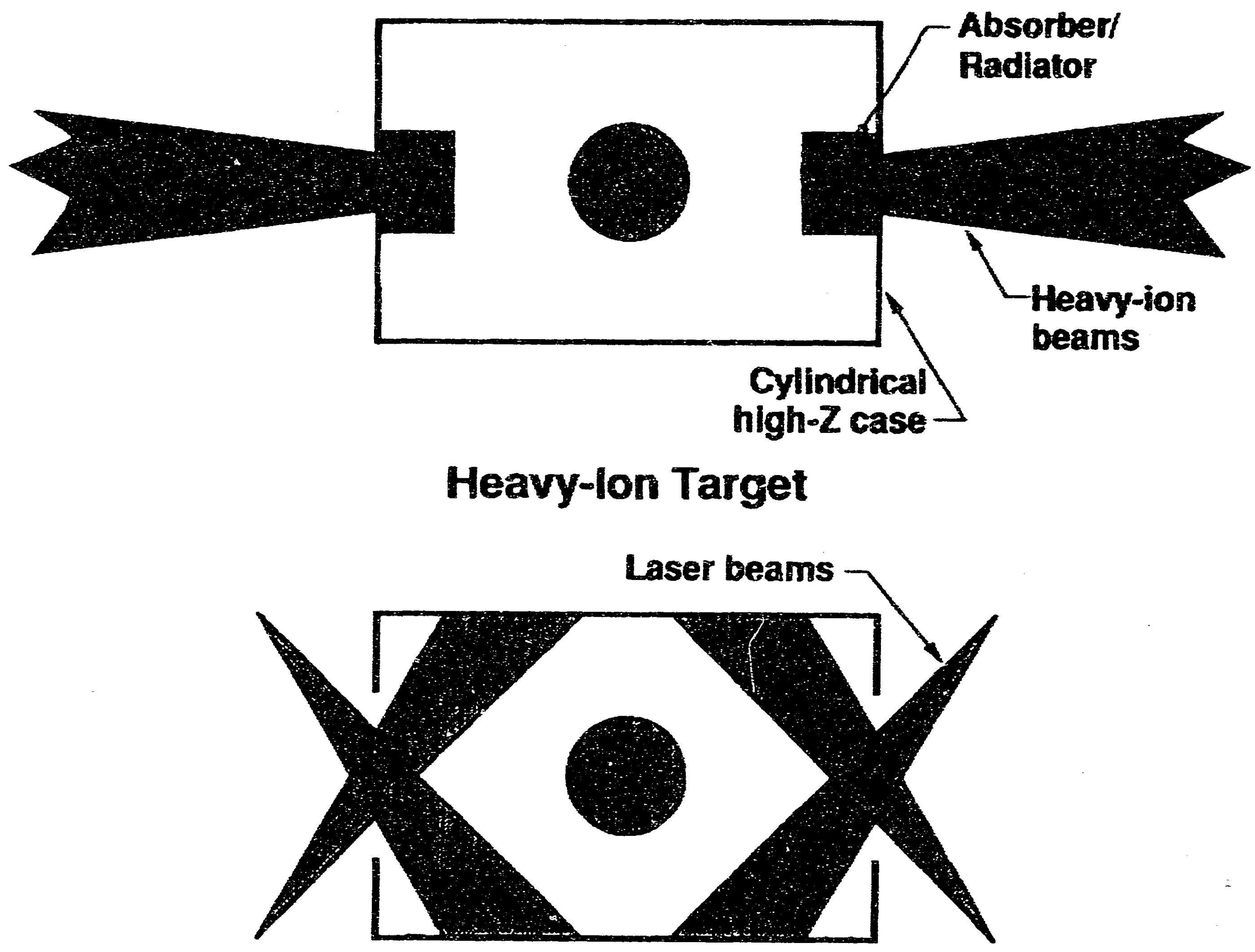

Figure 5

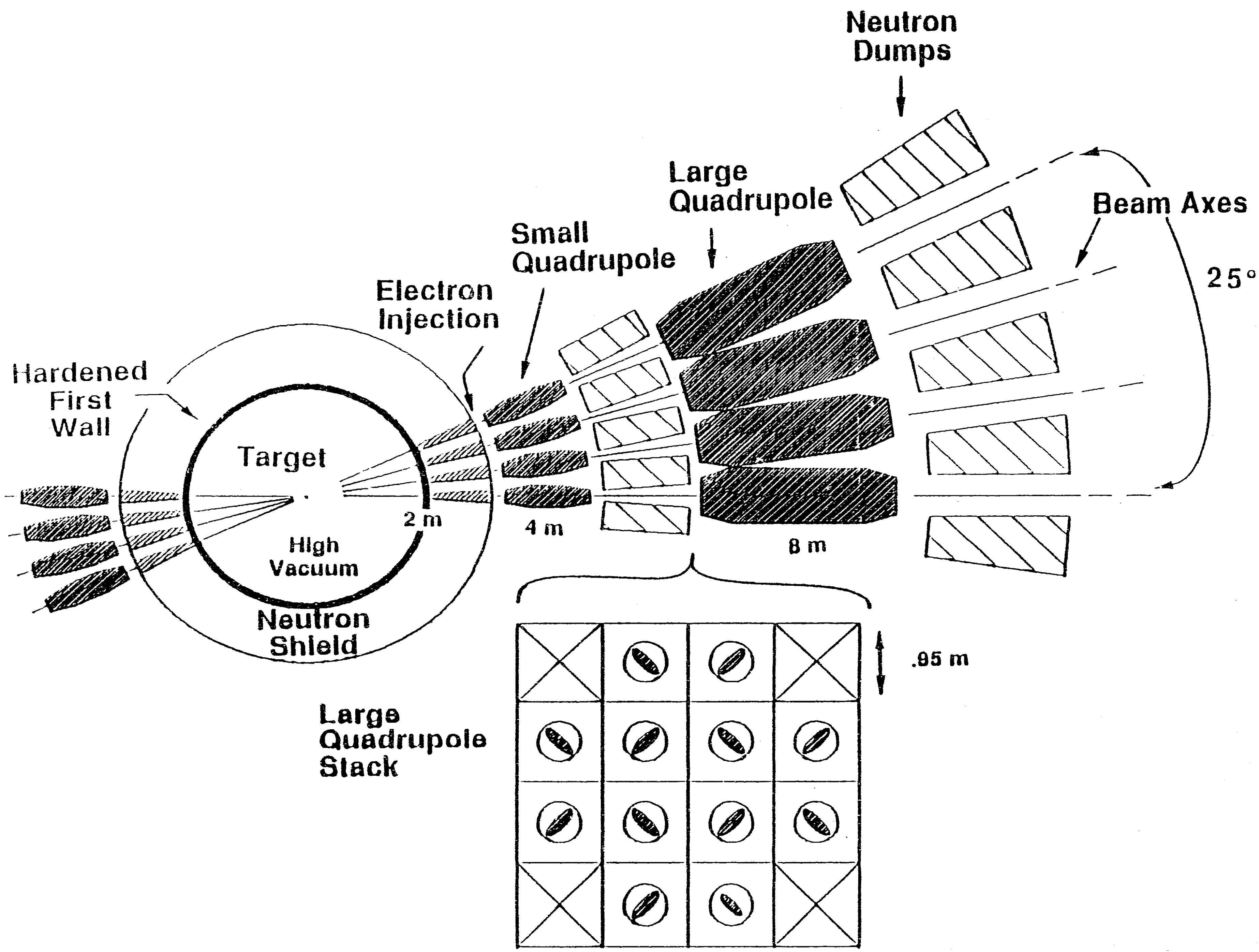
Neutron
Dumps
Large
Quadrupole
Beam Axes
25°
Small
Quadrupole
Electron
Injection
Hardened
First
Wall
Target
2 m
4 m
8 m
High
Vacuum
Neutron
Shield
.95 m
Large
Quadrupole
Stack

Figure 6

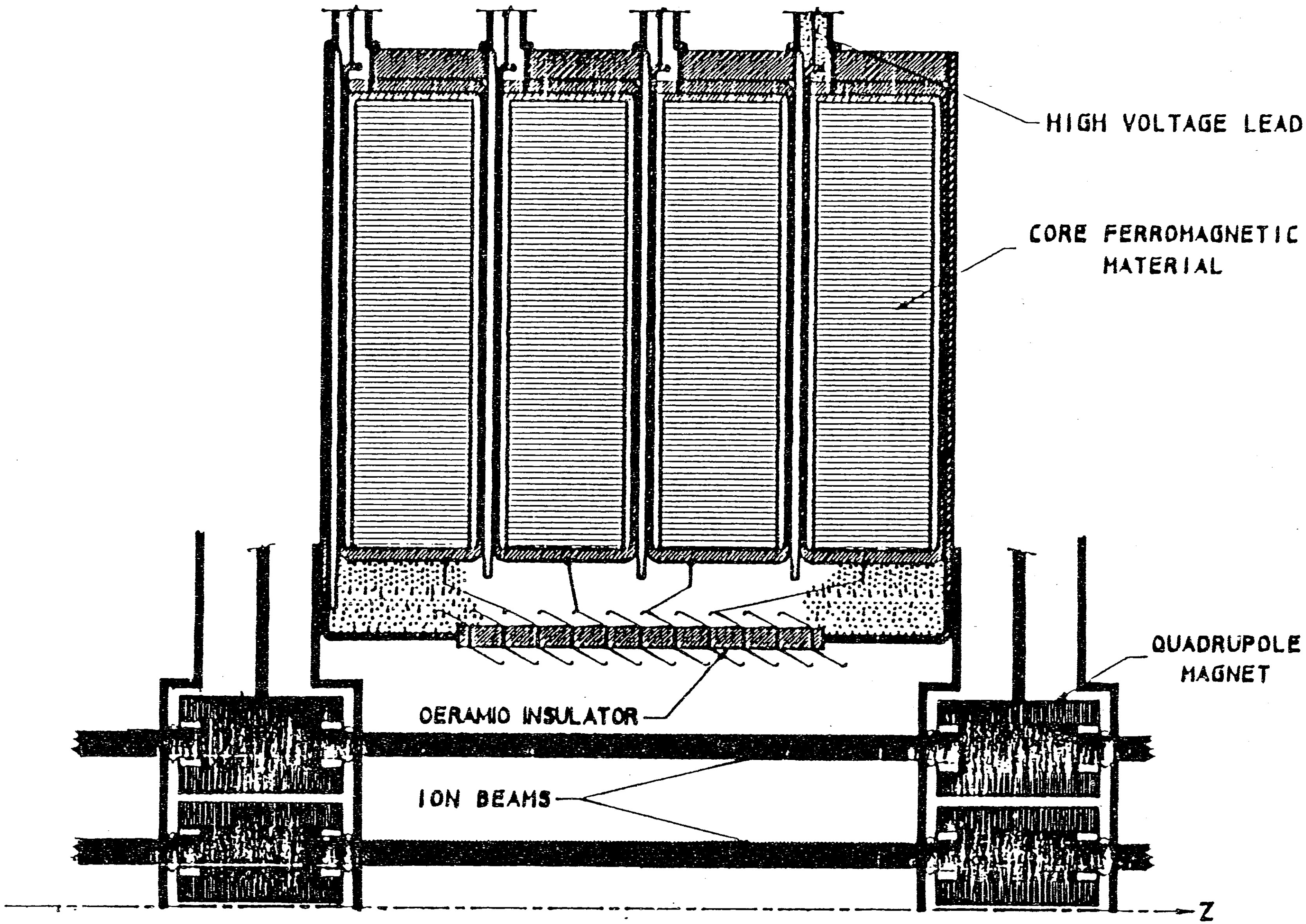
HIGH VOLTAGE LEAD
CORE FERROMAGNETIC
MATERIAL
QUADRUPOLE
MAGNET
CERAMIC INSULATOR
ION BEAMS
Z

Figure 7

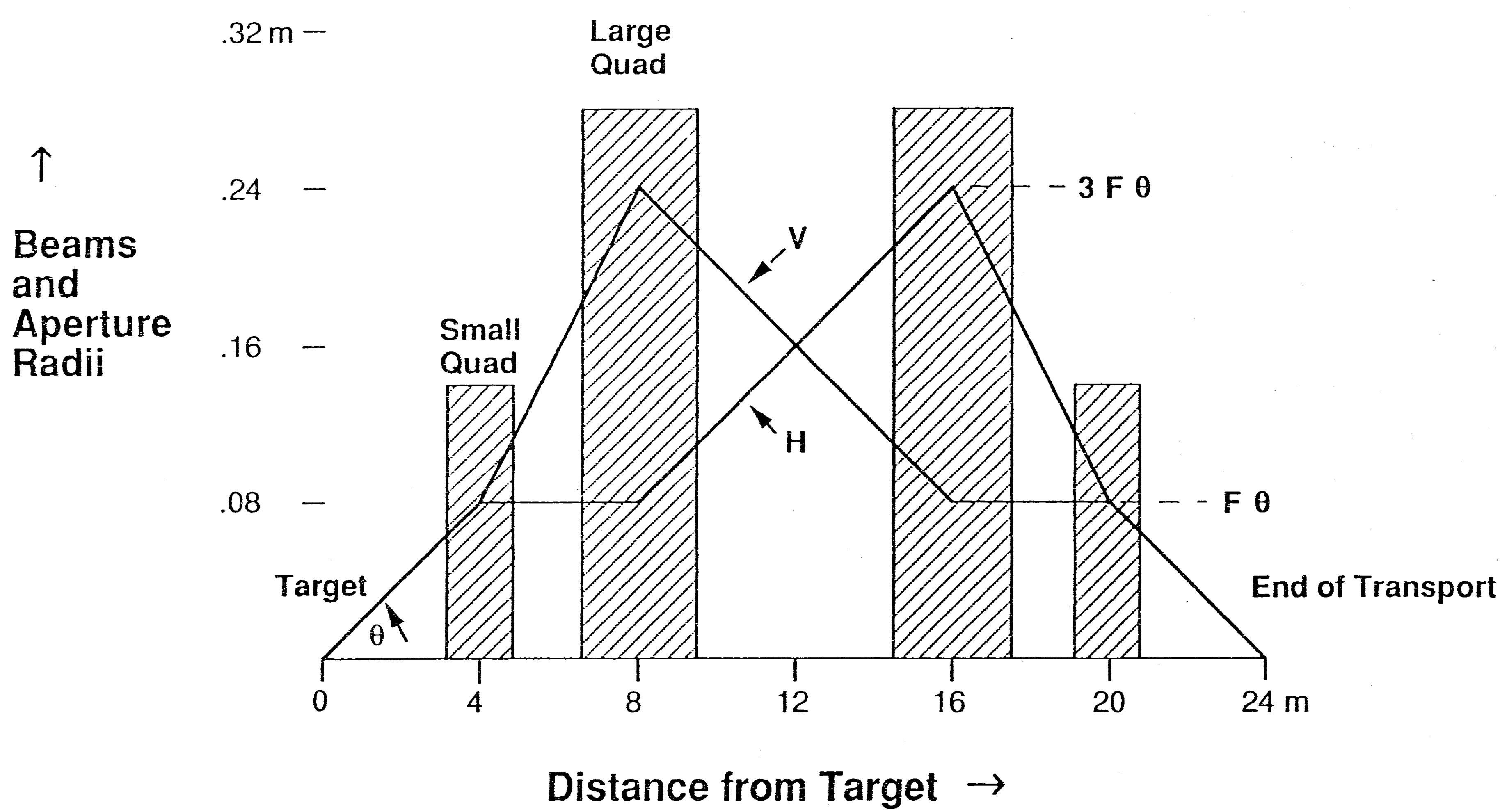
↑
Beams
and
Aperture
Radii
.32 m
.24
.16
.08
Large
Quad
Small
Quad
V
H
3 F θ
F θ
Target
θ
End of Transport
0
4
8
12
16
20
24 m
Distance from Target →

Figure 8

END

DATE FILMED

4/27/92